Journal of Applied Fluid Mechanics, Vol. 18, No. 3, pp. 641-660, 2025.
Available online at www.jafmonline.net, ISSN 1735-3572, EISSN 1735-3645.
https://doi.org/10.47176/jafm.18.3.2949

Thermal Behavior of Carboxymethyl Cellulose Containing Alumina Nanoparticles at the Entrance Region of an Annulus

F. Marzban [1, 2], M. Marzban [3], K. Mohammadzadeh [4†] and A. Abadeh [4]

[1] *Department of Mechanical Engineering, Yasouj University, Yasouj, Iran*
[2] *Department of Mechanical Engineering, Islamic Azad University Science and Research Branch, Tehran, Iran*
[3] *Department of Biomedical Engineering, Islamic Azad University Shahreza Branch, Shahreza, Iran*
[4] *Department of Mechanical Engineering, Arak University of Technology, Arak, Iran*

†*Corresponding Author Email*: k.mohammadzadeh@arakut.ac.ir

ABSTRACT

This paper investigates the thermal behavior of non-Newtonian nanofluids, specifically carboxymethyl cellulose (CMC) 0.5% and Al_2O_3 nanoparticles, in the fully developed region of a horizontal annulus. A three-dimensional axisymmetric, steady-state numerical solution is performed using the mixture multiphase model to compare with the results obtained from the single-phase model. The present study examines the effects of nanoparticle volume fraction ranging from 0.5% to 1.5% and particle diameters of 25 nm and 50 nm for various Reynolds numbers (Re) within the laminar flow regime. The results indicate that while the temperature profile distribution is slightly affected by changes in alumina concentration, significant variations are observed in the entrance region. Specifically, as Re is enhanced, the Nusselt number (Nu) is increased. For an outer wall heat flux of 1000 W/m² and a 1% concentration, Nu at the x/L = 0.25 section augments from 6.92 to approximately 13.14 as Re is enhanced from 5 to 500. Additionally, for the same conditions, Nu is about 0.78% higher for Al_2O_3 nanoparticles with a diameter of 25 nm than the ones with a diameter of 50 nm. In all cases, there is an acceptable agreement between the results obtained from the mixture and the single-phase models, with discrepancies of less than 1.13%.

Article History

Received June 30, 2024
Revised October 1, 2024
Accepted October 13, 2024
Available online January 1, 2025

Keywords:

CFD simulation
Carboxymethyl cellulose
Non-Newtonian nanofluids
Entrance region
Convective heat transfer

1. INTRODUCTION

Understanding the enhancement of convective heat transfer through an annulus is crucial in engineering applications, such as heat exchangers used in nuclear power systems (Jafarimoghaddam et al., 2017; Ahmad Khan & Altamush Siddiqui, 2020). Numerous researchers have investigated heat transfer enhancement in the thermal-entry region of an annulus using various approaches (Wen & Ding, 2004; Majid & Mohammad, 2017a). An approach to enhance heat transfer in thermal applications is to use fluids with increased thermal conductivity by adding high-thermal conductivity powders (Chon et al., 2005a; Vajjha & Das, 2009; Corcione, 2011; Sepehrnia et al., 2022a). Recent advancements in nanotechnology and nanoscience have led to the development of a new class of fluids known as nanofluids (Ellahi et al., 2015).

The thermal conductivity of particles in liquid suspensions is of significant interest in many engineering applications due to their enhanced thermal conductivity compared to base liquids, even at very low volume fractions (Akbar et al., 2016; Behroyan et al., 2016; Zarringhalam et al., 2016). Rabby et al. (2019) conducted a numerical study on laminar nanofluid flow using TiO_2, Al_2O_3, SiC, and CuO nanoparticles in the developed length of a heat pipe by employing the single-phase approach. Mojarrad et al. (2014) examined the hydrodynamic and thermal parameters of water–ethylene glycol (EG) and alumina nanofluids (WEG50) in the thermal developed region of a tube under constant wall temperature conditions experimentally. Additionally, they proposed a new correlation to predict Nu in the entrance length. Zeinali Heris et al. (2007a) demonstrated a thermal enhancement of approximately 3% in the developing region of a tube

Nomenclature

D_h	hydraulic diameter	q	heat flux
T_b	bulk temperature	r	radius
V_{Br}	Brownian velocity	u	axial velocity
d_{bf}	base fluid molecular diameter	x	axial coordinate
d_f	the equivalent diameter of a base fluid molecule	**Greek letters**	
d_p	nanoparticle diameter	α	thermal diffusivity
k_b	Boltzmann constant	$\dot{\gamma}$	shear rate
l_{bf}	base fluid mean free path	η	apparent viscosity (dimensionless)
r^*	radius ratio	μ	Viscosity
x^+	dimensionless length	π	Pi number
h	heat transfer coefficient	ρ	density
C	specific heat	ρ_{f_0}	the mass density of the base fluid
K	thermal conductivity	ϕ	nanoparticle volume fraction (dimensionless)
L	annulus length	**Subscripts**	
L_D	developing length	b	bulk
M	base fluid molecular weight	bf	base fluid
N	Avogadro number	ii	inner tube wall
Nu	Nusselt number	in	inlet
Pr	Prandtl number	m	mixture
Pe	Peclet number	nf	nanofluid
Re	Reynolds number	oo	outer tube wall
T	temperature	out	outlet
V	velocity	p	particle
k	consistency index	w	wall
n	power-law index (dimensionless)		

using water/Al_2O_3 nanofluid. They reported that the heat transfer coefficient (h) is approximately 1140 W/m²K when the volume fraction (ϕ) of Al_2O_3 is 2.5% and the Peclet number (Pe) is 6000.

The effects of convective heat transfer for non-Newtonian nanofluids in heat pipes have been studied by He et al. (2009) and Ragueb and Mansouri (2018). Hojjat et al. (2011b) experimentally assessed TiO_2, CuO, and Al_2O_3 nanoparticles suspended in CMC solution as a non-Newtonian base fluid, within a horizontal tube under a constant wall temperature boundary condition. They found that Nu is increased by 16%, 21%, and 19% for 1.5% concentrations of TiO_2, CuO, and Al_2O_3 nanoparticles, respectively, compared to the base fluid.

In an experimental investigation conducted by Shojaeian et al. (2017), Xanthan gum (XG) solutions, as non-Newtonian fluids, were used to examine convective heat transfer changes in the thermally developed region. They found that XG solutions are not ideal for enhancing convection heat transfer unless employed at low flow rates and volume fractions. At a flow rate of 44 ml/min, h was approximately 6000 W/m²K. Additionally, Siavashi and Rostami (2017a) evaluated natural convection of non-Newtonian nanofluids in a porous annulus using the mixture multiphase model.

In a numerical study, Rahimi et al. (2019) examined the impact of CuO nanoparticle diameter on velocity and temperature distributions in turbulent flow within a horizontal microtube containing 0.5% CMC. Using the finite volume method, they found that reducing the nanoparticle diameter from 50 to 25 nm increases the heat transfer coefficient by 0.34% at a constant amount of Re. In another numerical study, Al-Kouz et al., (2021) analyzed heat transfer and entropy generation in water-Fe_3O_4/CNT hybrid magnetic nanofluid flow using the Galerkin finite element method. Additionally, Abadeh et al. (2023) achieved a 23% augmentation in Nu by replacing water with ferrofluid in a micro-fin tube experimentally.

Hassan et al. (2018a) assessed the flow of water-based nanofluids over wavy surfaces in porous spherical packing beds, focusing on copper oxide particles. They employed the Dupuit-Forchheimer model to analyze the interactions between the fluid and porous walls. In a subsequent study, Marin et al. (2021) explored a nonlinear hyperbolic bioheat equation using the finite element method (FEM). Similarly, Vlase et al. (2017) utilized FEM to study the vibrations of mechanical bar systems.

Nasiri et al. (2011a) experimentally investigated the variations of Nu with Peclet number (Pe) in a turbulent flow regime within an annular duct for TiO_2-water and Al_2O_3-water nanofluids. They reported average values of approximately 74 and 73 for Nu for TiO_2 and Al_2O_3, respectively, at a 1.5% nanoparticle concentration for high values of Pe. Moghari et al. (2013) examined mixed convection under similar conditions and found that nanofluid distribution in the annular cross-section is non-uniform. Additionally, Beheshti et al. (2015) numerically

examined the convective heat transfer of TiO_2 -water and Al_2O_3-water nanofluids in a turbulent regime through an annular duct. For a 1.5% concentration and Re = 10,000, the average Nu was about 74 in experiments and 80 in the mixture model. Dawood et al. (2014, 2017) investigated heat transfer enhancement in an elliptic annulus using EG-based nanofluids. Naderi and Mohammadzadeh (2020) studied CuO-water nanofluid flow around an oscillating heated cylinder, observing h improvements ranging from 46% to 53.7%. Additionally, Davoudi et al. (2021) reported a modest enhancement of approximately 4% in the heat transfer rate for Al_2O_3-water and CuO-water nanofluids in a conical spiral heat exchanger.

Othman et al. (2019) analyzed the thermodynamic and conductive temperature of a fiber-reinforced thermoelastic medium, examining the effects of gravity in a new plane wave model. Siavashi and Jamali (2016b) studied the turbulent flow of TiO_2-water nanofluid through an annulus with varying radius ratios using the two-phase mixture model. Siavashi et al. (2017a) investigated the impact of porous ribs on the flow parameters of Al_2O_3-water nanofluid using the mixture multiphase model in an annulus. They found that for Re = 2000, ϕ = 5%, and a porous rib Darcy number (Da) of 0.1, Nu is approximately 75, compared to 60 in the absence of ribs. In the study by Benkhedda et al. (2018), the heat transfer enhancement of Ag-TiO_2-water hybrid nanofluid flow was investigated in a laminar regime through a horizontal annulus. Their results showed that the average Nu is increased by approximately 14% and 3.5% compared to pure water and TiO_2-water nanofluid, respectively, at a Grashof number (Gr) of 10^5. They also proposed a new correlation for calculating Nu for hybrid nanofluid flow. Bozorg et al. (2020) examined changes in flow parameters within a porous annulus. Their research indicated a 20%, 15%, and 42% increase in h, thermal efficiency, and pressure drop, respectively, with a porous structure with Da = 0.3. Bahiraei and Alighardashi (2016) demonstrated a 53% enhancement in the Bejan number by adding TiO_2 to a 0.5wt% CMC-water solution in a narrow annulus under a constant heat flux of 4000 W/m². In another study, Javadpour et al. (2017a) investigated the heat transfer characteristics of CuO nanoparticles in a 2wt% CMC non-Newtonian nanofluid flowing through an annulus, finding a 14.7% increase in h at a 0.5% concentration compared to pure water. Siavashi and Rostami (2017b) numerically examined free convection of non-Newtonian nanofluid in an annulus using the mixture model.

Hassan et al. (2018b) studied the hydrothermal properties of Cu–Ag/water hybrid nanofluids, comparing them with mono nanofluids, i.e., Cu/water and Ag/water. Shahsavar et al. (2018) investigated the CNT-Fe_3O_4 hybrid nanofluid in glycerol-based non-Newtonian fluid within a concentric annulus. They observed an approximately 85% reduction in h on the inner tube wall and a 35% enhancement on the outer tube wall with 1.1% CNT and 0.7% Fe_3O_4 nanoparticle volume fractions. Sepehrnia et al. (2022b) empirically examined the rheological properties of a ZnO/MWCNT (30/70) hybrid nanoparticle in engine oil as a non-Newtonian nanofluid. Ghanbari and Javaherdeh (2020) experimentally demonstrated a 40% increase in the heat transfer coefficient by adding 0.2wt% nano porous graphene to a CMC solution. Additionally, Yarmohammadi et al. (2020) reported a 33% enhancement in heat transfer in a corrugated tube compared to a smooth tube using the artificial neural network (ANN) algorithm.

Due to the significance of nanofluids in engineering research and thermal sciences and their applications in industries, such as heat exchangers and electronic equipment cooling, this study focuses on annular geometry. Although extensive research has been conducted on heat transfer in annular geometries for both Newtonian and non-Newtonian fluids, there are limitations in simulating carboxymethyl cellulose nanofluids using multiphase methods. This study uses the two-phase mixture numerical method to assess the nanofluid behavior and compares the results with those obtained from a valid single-phase model. The objectives are to examine the accuracy of multiphase numerical methods for non-Newtonian nanofluids and to analyze thermal parameters, including changes in the heat transfer coefficient in the entrance region. Additionally, the research examines temperature distribution and Nu variations in laminar flows, considering the rheology of non-Newtonian fluids.

2. NUMERICAL MODELING

2.1. Modeling Geometry

The present work examines the forced convection of a 0.5% CMC/Al_2O_3 non-Newtonian nanofluid inside a horizontal annulus with constant wall heat flux. Figure 1 illustrates the schematic of the simulated axisymmetric 3D geometry and applied boundary conditions. The effective thermal conductivity and viscosity of the non-Newtonian nanofluid are considered as functions of nanoparticle diameter and nanofluid temperature. The single-phase model is considered to model fine solid particles (<100 nm), specifically 25 nm and 50 nm. The annulus has a length of 2.8 m and a radius ratio ($r^*=r_{in}/r_{out}$) of $r^* = 0.5$, where inner and outer tube diameters are 8 mm and 16 mm, respectively.

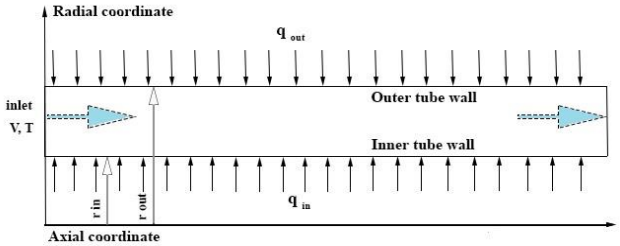

Fig. 1 Schematic of the simulated geometry

2.2. Governing Equations

2.2.1. Single-Phase Model

The non-Newtonian nanofluid flow is assumed to be incompressible, laminar, and steady-state. Consequently, the governing equations within a single-phase framework are expressed as follows (Moraveji et al., 2012):

Continuity equation:

$$\nabla.(\rho_{nf}V_m) = 0 \tag{1}$$

Momentum equation:

$$\nabla.(\rho_{nf}V_mV_m) = -\nabla P + \nabla.(\mu_{nf}\nabla V_m) \tag{2}$$

Energy equation:

$$\nabla.(\rho_{nf}CV_mT) = \nabla.(\mathrm{k}_{nf}\nabla T) \tag{3}$$

2.2.2. Mixture Model

The two-phase mixture approach is utilized to analyze the thermal performance of the nanofluids. In this model, the mixture is treated as a single two-phase fluid, where a specific fraction of each phase is present within a given control volume. Each phase has its own velocity vector. The governing equations for the mixture model framework are as follows (Bianco et al., 2010; Lotfi et al., 2010; Mokhtari Moghari et al., 2011a; Rabienataj Darzi et al., 2016; Kumar & Sarkar, 2018):

Continuity equation:

$$\nabla\cdot\left(\rho_m\vec{V}_m\right) = 0 \tag{4}$$

Momentum equation:

$$\nabla.\left(\rho_m\vec{V}_m\vec{V}_m\right) = -\nabla p + \nabla.\left(\mu_m\nabla\vec{V}_m\right) + \nabla.\left(\sum_{k=1}^{n}\phi_k\rho_k\vec{V}_{dr,k}\vec{V}_{dr,k}\right) \tag{5}$$

Energy equation:

$$\nabla.\ \sum_{k=1}^{n}(\rho_kC_{p,\mathrm{k}}\phi_k\vec{V}_kT) = \nabla.\ (k_m\nabla T) \tag{6}$$

Volume fraction equation:

$$\nabla.\left(\phi_p\rho_p\vec{V}_m\right) = -\nabla.\left(\phi_p\rho_p\vec{V}_{dr,p}\right) \tag{7}$$

where ρ_m and $\vec{V}_m$ are the mixture density and velocity, respectively (Siavashi & Jamali, 2016a; Siavashi et al., 2017b).

$$\vec{V}_{\mathrm{m}} = \frac{\sum_{k=1}^{n}(\phi_k\rho_k\vec{V}_k)}{\rho_m} \tag{8}$$

For the two-phase model:

$$\vec{V}_m = \frac{(1-\phi)\rho_p\vec{V}_p+\phi\rho_s\vec{V}_s}{\rho_{\mathrm{m}}} \tag{9}$$

Here, p and s indices denote the primary and secondary phases, respectively. In the present study, the primary phase is the base fluid, and the secondary phase is nanoparticles.

In Eq. (7), $\vec{V}_{dr,k}$ refer to the drift velocity of the secondary phase k, which is associated with relative velocity,

$$\vec{V}_{dr,p} = \vec{V}_{sp} - \sum_{k=1}^{n}\frac{\phi_k\rho_k}{\rho_{\mathrm{m}}}\vec{V}_{pk} \tag{10}$$

where $\vec{V}_{sp}$ is slip velocity which is defined as:

$$\vec{V}_{sp} = \vec{V}_s - \vec{V}_p \tag{11}$$

The slip velocity is calculated using Eq. (12), developed by Manninen and Taivassalo (1996).

$$\vec{V}_{sp} = \frac{\rho_pd_p^2}{18\,\mu_f f_{drag}}\frac{(\rho_{\mathrm{m}}-\rho_p)}{\rho_p}\vec{a} \tag{12}$$

The acceleration ($\vec{a}$) is:

$$\vec{a} = \vec{g} - \left(\vec{V}_{\mathrm{m}}.\nabla\right)\vec{V}_m - \frac{\partial\vec{V}_m}{\partial t} \tag{13}$$

where $\vec{g}$ is gravity acceleration, which is enforced in the y-direction. f_{drag} denotes the drag coefficient. There are several correlations available in the literature that fit f_{drag} as a function of the Re_p. Here, Eq. (14) introduced by Schiller and Naumann is used to determine f_{drag} as follows (Mokhtari Moghari et al., 2011b):

$$f_{drag} = \begin{cases} 1 + 0.15\ \mathrm{Re}_p^{0.687} & \mathrm{Re}_p \le 1000 \\ 0.0183\ \mathrm{Re}_p & \mathrm{Re}_p > 1000 \end{cases} \tag{14}$$

where $Re_p = \frac{V_md_p}{\upsilon_m}$

2.3. Boundary Conditions

Due to the annular geometry depicted in Figure 1, effective parameters are applied to its boundaries. The boundary conditions are detailed in Table 1. Notably, the ratio of q_{in}/q_{out} is set to 0.5 and 1, indicating that the outer surface is subjected to a constant heat flux that is a reference parameter for the thermal conditions.

2.4. Physical and Thermal Properties of Nanofluids

CMC, derived from cellulose, exhibits as a non-Newtonian pseudoplastic fluid in its aqueous solution

Table 1 Boundary conditions

Boundary	Type of boundary condition
Inlet	Uniform velocity ($V_{ave,in} = 0.05, 0.22, 1.03\ \frac{m}{s}$) Uniform temperature ($T_{in} = 300\ K$)
Inner surface of the tube wall	No-slip Uniform wall heat flux (q_{in}) ($q^{"} = 500, 1000\ \frac{w}{m^2}$)
Outer surface of the tube wall	No-slip Uniform wall heat flux (q_{out}) ($q^{"} = 1000\ \frac{w}{m^2}$)
Outlet	Atmospheric static pressure

(Soltani et al., 2010). It is assumed that the base fluid and nanoparticles are in thermal equilibrium and flow with the same velocity. The following expressions are used to calculate the thermo-physical properties of the non-Newtonian nanofluid under study.

The density of the nanofluid is calculated as (Akbari et al., 2015; Tahiri & Mansouri, 2017):

$$\rho_{nf} = \phi\rho_p + (1-\phi)\rho_{bf} \tag{15}$$

The specific heat of nanofluids is computed using Eq. 16 (Rea et al., 2009; Popa et al., 2017; Javadpour et al., 2018):

$$C_{nf} = \frac{(1-\phi)(\rho C)_{bf} + \phi(\rho C)_p}{(1-\phi)\rho_{bf} + \phi\rho_p} \tag{16}$$

There are various correlations and models to estimate the nanofluid thermal conductivity (k_{nf}) in the literature (Heris et al., 2006; ; Moghadassi et al., 2009; Azmi et al., 2012; Mirzaei & Azimi, 2016; Majid & Mohammad, 2017b; Heidarshenas et al., 2020). However, the following correlation is employed for calculating K_{nf} (Lelea, 2011; Sajadifar et al., 2017), which considers the Brownian motion and the nanoparticle mean diameters (Chon et al., 2005b).

$$k_{nf} = f(T) \tag{17}$$

$$\frac{k_{nf}}{k_{bf}} = 1 + 64.7(\phi)^{0.7460}\left(\frac{d_{bf}}{d_p}\right)^{0.3690}\left(\frac{k_p}{k_f}\right)^{0.7476} Pr^{0.9955} Re_{np}^{1.2321} \tag{18}$$

where ϕ denotes the volume concentration of nanoparticles of diameter d_p with thermal conductivity of k_p, suspended in the base fluid with a molecular diameter of d_{bf} and thermal conductivity of k_{bf}. The Prandtl number (Pr), and Re are respectively defined as:

$$Pr \equiv \frac{\mu}{\rho_{bf}\alpha} = \frac{C_{p_{bf}}\mu_{bf}}{k_{bf}} \tag{19}$$

and

$$\mathrm{Re}_{np} \equiv \frac{\rho_{bf}V_{Br}d_p}{\mu} = \frac{\rho_{bf}k_bT}{3\pi\mu^2 l_{bf}} \tag{20}$$

where l_{bf} is the base fluid mean free path, k_b denotes the Boltzmann constant (k_b=1.3807 × 10^{-23} J/K), and μ is the viscosity of the base fluid, which is determined as (Rahimi Gheynani et al., 2019):

$$\mu = 2.414 \times 10^{-5} \times 10^{247.8/(T-140)} \tag{21}$$

V_{Br} is nanoparticles Brownian velocity based on the Einstein diffusion theory:

$$V_{Br} \equiv \frac{k_bT}{3\pi\mu d_p l_{bf}} \tag{22}$$

The power-law model is employed to investigate the performance of the base fluid (Hojjat et al., 2011a):

$$\tau = K\dot{\gamma}^n \tag{23}$$

$$\eta = K\dot{\gamma}^{n-1} \tag{24}$$

Here, $\dot{\gamma}$ is the shear rate, η is the apparent viscosity, and K and n are the consistency index and the power-law index, respectively. Despite various models to calculate the nanofluid viscosity (Masoumi et al., 2009; Mishra et al., 2014; Koca et al., 2018), the Corcione correlation (Corcione, 2011) is considered in this paper.

$$\mu_{nf} = f(\dot{\gamma}) \tag{25}$$

$$\frac{\mu_{nf}}{\mu_f} = \frac{1}{1-34.87(d_p/d_f)^{-0.3}\phi^{1.03}} \tag{26}$$

where,

$$d_f = 0.1\left(\frac{6M}{N\pi\rho_{f_0}}\right)^{\frac{1}{3}} \tag{27}$$

where M denotes the base fluid molecular weight, N stands for the Avogadro number ($N = 6.022 \times 10^{23}\ \left(\frac{1}{kmol}\right)$), and ρ_{f_0} is the base fluid density computed at T_0 = 293 K.

In this study, Re and Pr are computed as (Hojjat et al., 2011c):

$$\mathrm{Re} = \frac{\rho u^{2-n} D_h^n}{K} \tag{28}$$

$$Pr = \frac{Cp_{nf}.K}{k_{nf}}\left(\frac{u}{D_h}\right)^{n-1} \tag{29}$$

The thermo-physical properties of the nanofluids are computed based on Eqs. (15) and (16) for nanofluid density and specific heat, respectively. Additionally, Eq. (18) is used to calculate the nanofluid thermal conductivity. These properties are summarized in Table 2 (Akbari et al., 2017).

2.5. Validation

To validate the results obtained from the numerical approaches, the heat transfer coefficient for nanofluid flow in a circular tube under constant heat flux in the developed

Table 2 The thermophysical properties of nanofluids

Nanofluid	$\rho\ (\frac{m^3}{kg})$	$C_p\ (\frac{J}{kg\ K})$	$k\ (\frac{W}{m\ K})$	
			$d_p = 25nm$	$d_p = 50nm$
CMC (0.5%) + 0.5% Al_2O_3	1011.865	4112.0267	0.6310	0.6269
CMC (0.5%) + 1.0% Al_2O_3	1026.730	4046.9927	0.6433	0.6364
CMC (0.5%) + 1.5% Al_2O_3	1041.595	3983.8150	0.6539	0.6447

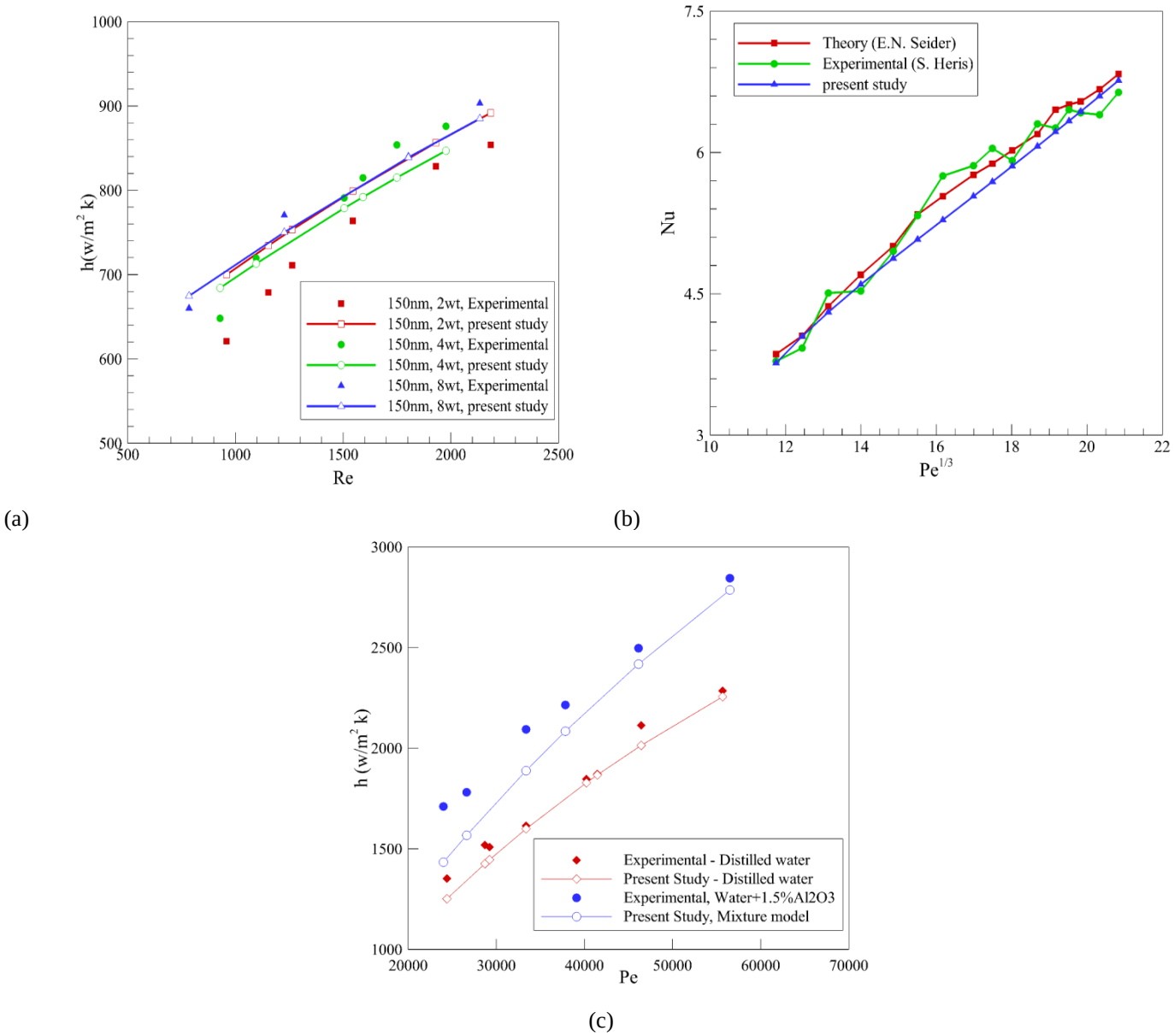

(a) (b)

(c)

Fig. 2 Comparison between the results obtained from the simulations and those reported in previous studies: (a) h vs. Re; (b) Nu vs. $Pe^{1/3}$; (c) h vs. Pe

region is compared with experimental data reported by Anoop et al. (2009). Additionally, changes in Nu based on the cube root of Pe are analyzed based on the experimental study of Zeinali Heris et al. (2007b). The comparison results are presented in Figs 2a and 2b, respectively. As shown in these figures, there is a good agreement between the simulation results of the current study and those from previous studies, with a maximum discrepancy of 8%.

Furthermore, the experimental results of Nasiri et al. (2011b) are modeled using the mixture multiphase approach. They investigated the heat transfer parameters for distilled water with various concentrations of Al_2O_3 nanoparticles in turbulent flow inside an annulus under a constant temperature boundary condition. The data obtained from the mixture model simulation for water with 1.5% Al_2O_3 show an acceptable average difference of about 8% compared to the experimental results (see Fig. 2c).

2.6. Modeling Approach

The governing equations are discretized using the finite volume method. The SIMPLE algorithm is employed to couple pressure and velocity fields, while the momentum and energy equations are discretized utilizing the second-order upwind scheme (Mohammadzadeh et al., 2018). The convergence criterion for all conservation equations is set to 10^{-14}.

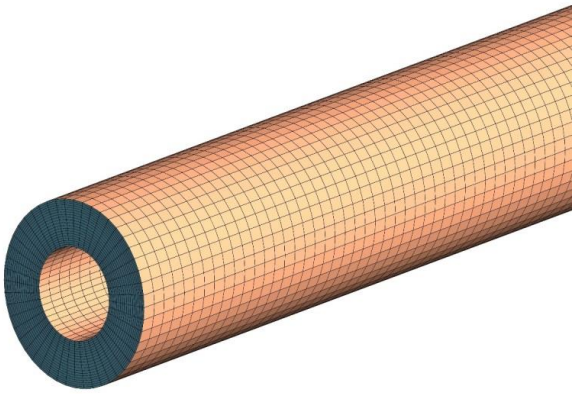

Fig. 3 Computational grid with 20×2800 cells

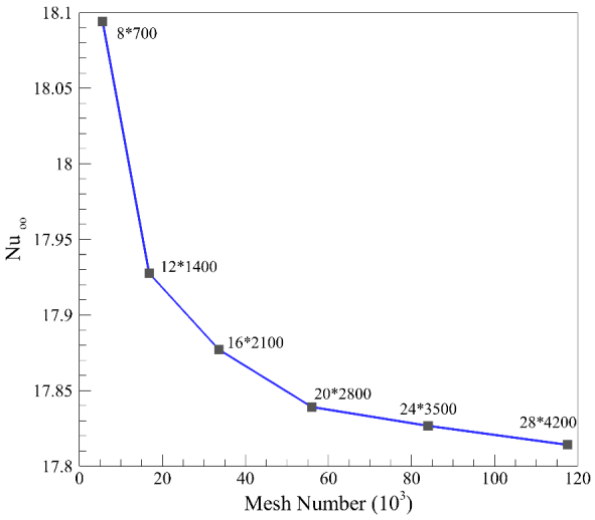

Fig. 4 Grid independence test

2.7. Grid Independency

In the discretization process, to achieve accurate results near the tube walls and along the entrance region, the grids in the radial and axial directions are non-uniform. The grid is finer in areas near the annulus inlet and close to the walls, where the velocity and temperature gradients are most significant (see Fig. 3). To ensure that the results are not dependent on grid size, simulations are conducted using several grid resolutions. The amount of Nu at the outer tube wall is calculated using six grids, as shown in Fig. 4. Since the difference between the results obtained with a grid with 20×2800 cells and the finest grid is approximately 0.14%, the 20×2800 grid resolution is chosen as the grid for further simulations.

3. Results And Discussions

The simulation results are given for various Re (5, 50, 100, 250, 500, 1000, and 2000), nanoparticle volume fraction ($\phi = 0.5, 1,$ and $1.5\ wt\%$), wall heat flux ($q_{in}/q_{out} = 0.5$ and 1) and particle diameters ($dp =$ 25 and $50\ nm$). After the convergence of the numerical solution, the local h (Zeinali Heris et al., 2007c), local Nu (Javadpour et al., 2017b) can be determined at the inner and outer tube walls using Eqs (30) to (33), respectively.

$$h_{ii} = \frac{q_{wi}}{(T_{wi} - T_b)} \tag{30}$$

$$h_{oo} = \frac{q_{wo}}{(T_{wo} - T_b)} \tag{31}$$

$$Nu_{ii} = \frac{h_{ii}\, D_h}{k_{nf}} \tag{32}$$

$$Nu_{oo} = \frac{h_{oo}\, D_h}{k_{nf}} \tag{33}$$

3.1 Thermal Analysis

The effects of critical factors, such as Re, ϕ, and heat flux, on thermal behavior of nanofluids are investigated. Figure 5 presents the dimensionless temperature distribution at various cross-sections along the developed region for $Re = 500$ and $q_{in} = 500\ \frac{W}{m^2}$. The results show that the temperature profile undergoes minimal changes at the entrance length, as the nanofluid flow is not significantly influenced by the heat flux in this region. Additionally, due to insufficient development of the thermal boundary layer at the entrance length (Fig. 5a), a substantial thermal gradient ($\partial T/\partial r$) is observed near the inner and outer walls of the annulus.

The numerical results reveal that small variations in the thermal gradient occur near the annulus surface by changing ϕ and nanoparticle diameter. For $q_{in}/q_{out} = 0.5$, the heat flux on the outer surface of the annulus is twice that the one on the inner surface, resulting in a higher thermal gradient adjacent to the outer wall compared to the inner surface (see Fig. 5). Conversely, for $q_{in}/q_{out} = 1$, the temperature gradient on the inner annulus wall is significantly higher than that for $q_{in}/q_{out} = 0.5$.

Furthermore, at a given Re, the dimensionless temperature profile across different sections of the developed region shows similar behavior at various amounts of ϕ. These variations are illustrated in Fig. 6 for Re = 500.

Another notable result is that, despite applying equal amounts of heat flux to both walls ($q_{in}/q_{out} = 1$), the temperature distribution and corresponding temperature gradient are not symmetrical. This asymmetry arises because the outer wall of the annulus has a larger surface area in contact with the flow, allowing more energy to be transferred from the wall to the adjacent fluid. Consequently, this results in a more pronounced temperature gradient. Thus, the temperature distribution

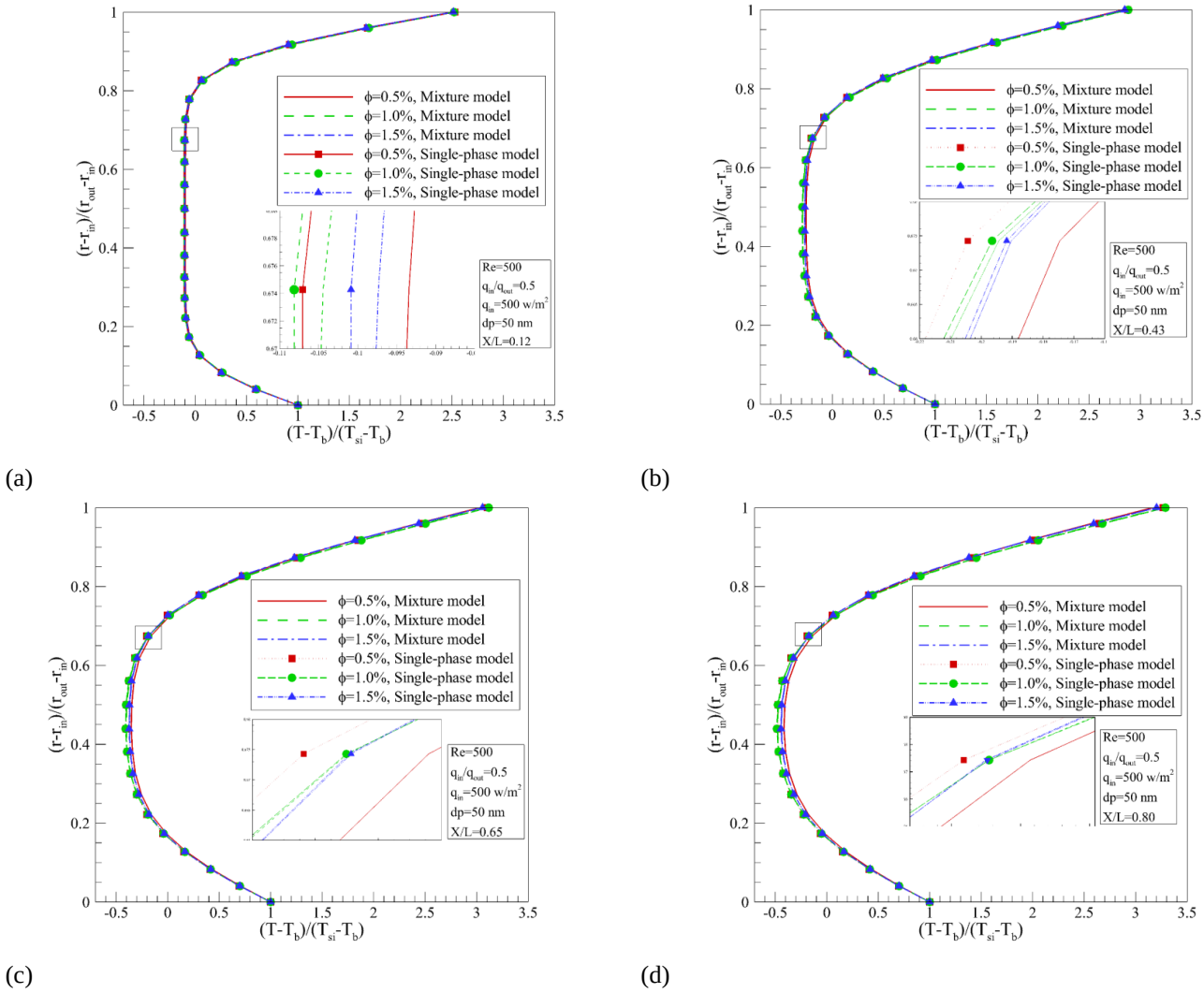

Fig. 5 Dimensionless temperature profiles at different axial positions (a) x/L = 0.12; (b) x/L =0.43; (c) x/L = 0.65; and (d) x/L = 0.8

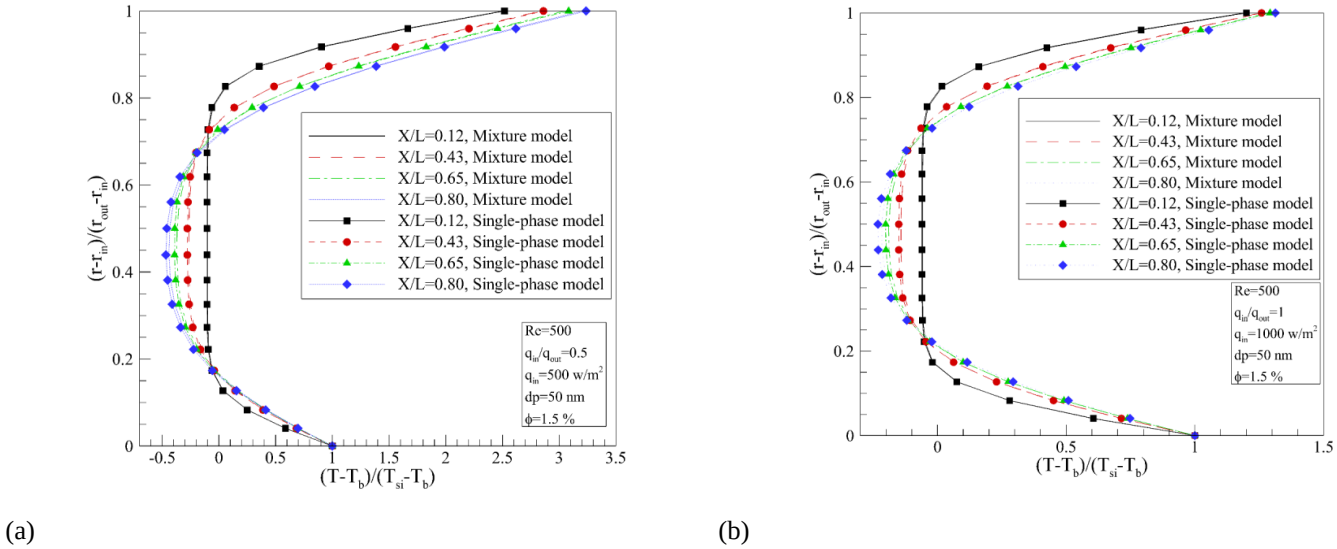

Fig. 6 Dimensionless temperature profiles at different axial positions when $\mathrm{Re} = 500, dp = 50\ \mathrm{nm}, \phi = 1.5\%$ for (a) $q_{in}/q_{out} = 0.5$ and (b) $q_{in}/q_{out} = 1$

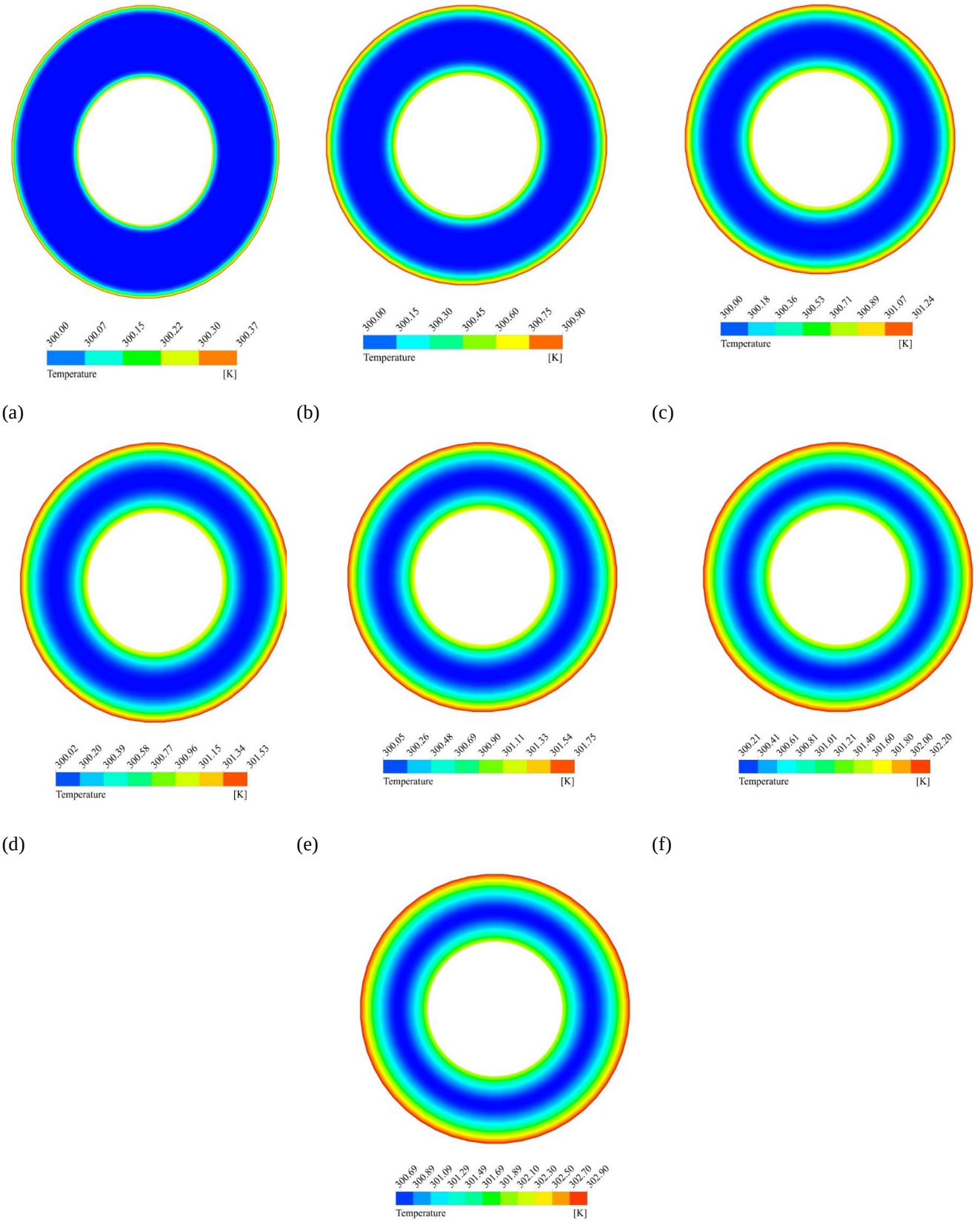

Fig. 7 Variations of the local temperature (a) $x = 0.01$ m; (b) $x = 0.105$ m; (c) $x = 0.252$ m; (d) $x = 0.436$ m; (e) $x = 0.620$ m; (f) $x = 1.105$ m; and (g) $x = 2.1$ m; ($\mathrm{Re} = 50, \phi = 1\%, dp = 50$ nm, $q_{in}/q_{out} = 1$)

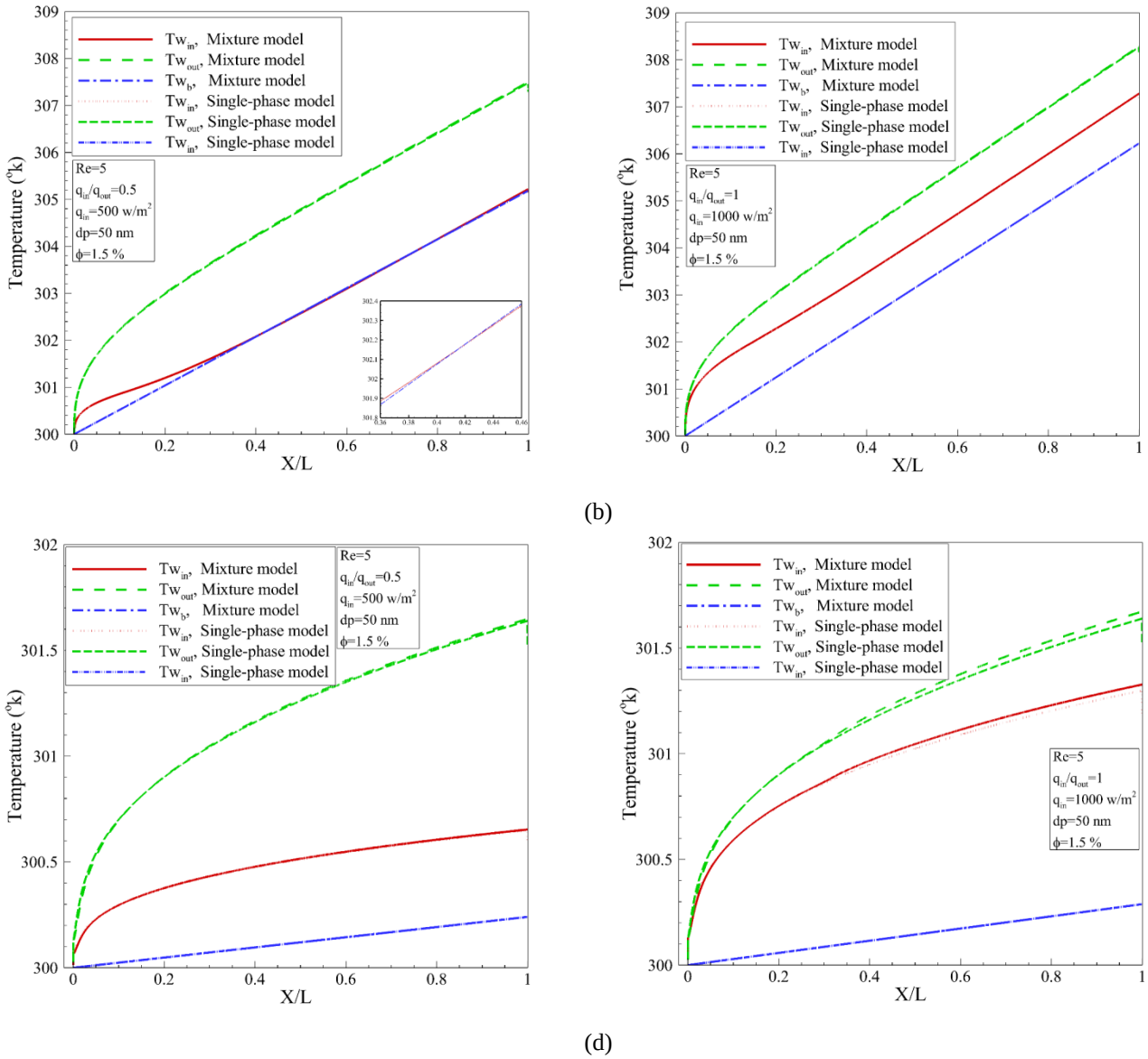

Fig. 8 Axial evolution of bulk, inner, and outer tube wall temperature for (a) Re $= 5, q_{in}/q_{out} = 0.5$; (b) Re $= 5, q_{in}/q_{out} = 1$; (c) Re $= 500, q_{in}/q_{out} = 0.5$; and (d) Re $= 500, q_{in}/q_{out} = 1$

becomes asymmetric across different sections. Figure 7 confirms this by showing the fluid temperature distributions and the growth of the thermal boundary layer along the length of the annulus.

In this section, temperature variations along the annulus walls and the fluid bulk temperature are examined. Figure 8 demonstrates that significant temperature changes occur from the annulus entrance up to x/L=0.12, indicating substantial thermal development within this region. Additionally, as noted, at lower values of Re, the outer wall has a larger surface area compared to the inner one, allowing more energy to be transferred to the outer wall. Consequently, the outer wall temperature is higher than that of the inner wall.

Figure 8 illustrates that the outer wall temperature is approximately 305 K and the bulk fluid temperature is slightly above 303 K at the middle of the developed region $(x/L = 0.5)$ for a heat flux of $q_{in} = 1000\ W/m^2$ and $Re = 5$. In contrast, at Re = 500, the temperatures at the same section are 301.3 K for the outer wall and 300.45 K for the bulk fluid.

In all cases, the bulk temperature is enhanced linearly but remains lower than the inner wall temperature along the annulus. Higher amounts of Re result in a greater temperature difference between the wall and the bulk fluid. Additionally, increasing the heat flux to 1000 W/m^2 with $q_{in}/q_{out} = 1$ reduces the temperature difference between the inner and outer walls.

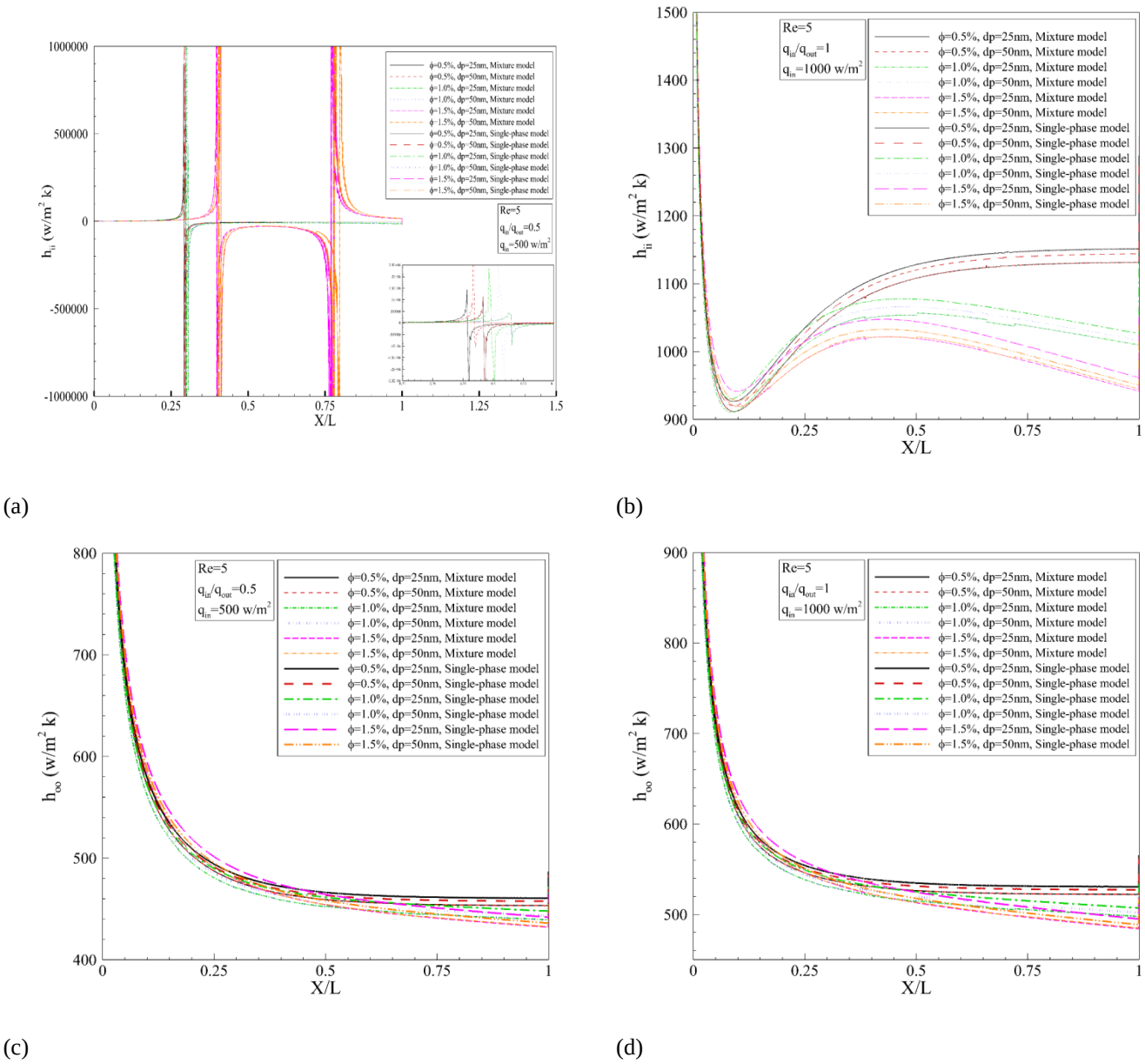

Fig. 9 Axial variations of h at the inner and outer tube walls for $= 5$: (a, c) $q_{in}/q_{out} = 0.5$; (b, d) $q_{in}/q_{out} = 1$

The changes in h depend entirely on the changes in the wall temperature and its difference with the nanofluid bulk temperature. Therefore, in the annulus section for Re=5, in which the inner wall-to-bulk temperature difference reaches a negligible value, the values of h and, as a result, Nu experience a significant increase. As X/L is enhanced, this trend changes in such a way that the value of h becomes negative when the bulk temperature is slightly higher than the inner wall temperature, in which case heat is transported from the fluid flow to the inner wall because the fluid flow is more affected by the outer wall (see Fig. 8.a, Fig. 9.a, and Fig. 11.a).

Due to the significant temperature difference between the outer wall and the bulk fluid, the heat transfer coefficients (h_{ii} , h_{oo}) exhibit a similar trend along the developed region. Specifically, these coefficients show a decreasing trend, starting from a maximum value at the entrance and then approaching a constant value as the flow develops (see Fig. 10a), similar to the behavior observed in Newtonian fluid flow.

It should also be noted that increasing the heat flux on the outer wall to 1000 W/m^2 ($q_{in}/q_{out} = 1$) results in an initial decrease followed by a relative increase in h (see Fig. 9b). The numerical results indicate that while increasing the nanoparticle volume fraction initially enhances h on the inner wall at the entrance region, this effect declines along the annulus length. For example, at $Re = 5$ and $q_{in} = 1000\ W/m^2$, h on the inner wall is

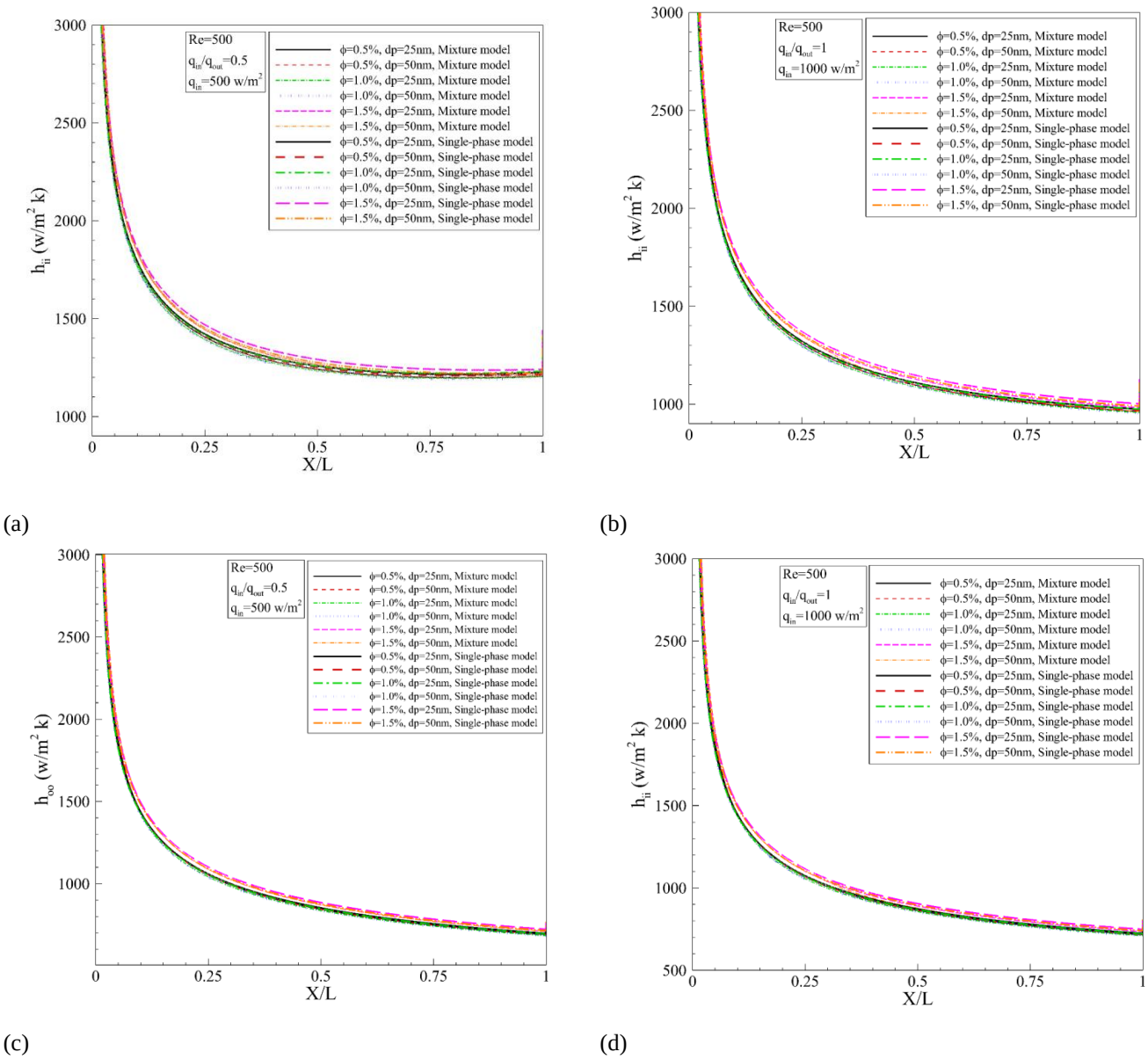

Fig. 10 Axial variations of h at the inner and outer tube walls for Re = 500: (a, c) $q_{in}/q_{out} = 0.5$; (b, d) $q_{in}/q_{out} = 1$

1047 W/m²K at x/L=0 for ϕ=1.5%, compared to 1018 W/m²K for ϕ=0.5. By at x/L=1, h increases to 1329 W/m²K for ϕ=1.5%, which is approximately 20% higher than 1078 W/m²K for ϕ=0.5%. In contrast, the heat transfer coefficient on the outer wall exhibits a similar, smooth trend throughout the developed region.

Furthermore, an augmentation in the nanoparticle diameter from 25 nm to 50 nm leads to a minor decrease in h and, consequently, in Nu. For instance, at Re=5 and $q_{in} = 1000\ W/m^2$, h is decreased from 1018 W/m²K for d_p=25nm to 1013 W/m²K for d_p =50 nm.

As illustrated in Fig. 11, Nu increases with Re, particularly for a heat flux of q_{in}=1000 W/m^2 and ϕ = 0.01. Nu_{oo} rises from 6.92 at x/L=0.25 to approximately 13.14, nearly doubling as Re increases from 5 to 500.

As shown in Fig. 11, reducing the heat flux on the inner wall from 1000 W/m^2 to 500 W/m^2 results in a minor decrease in Nu_{oo}, from 13.14 to 13.10 at Re=500. In contrast, a more substantial decrease is observed in Nu_{ii}, which drops from 17.62 to 16.14.

3.2 Developed Region

The length of the developed region is characterized by the dimensionless parameter x^+, measured from the annulus inlet, as defined by Hojjat et al. (2011d):

$$x^+ = \frac{2x/D_h}{Re.Pr} \tag{34}$$

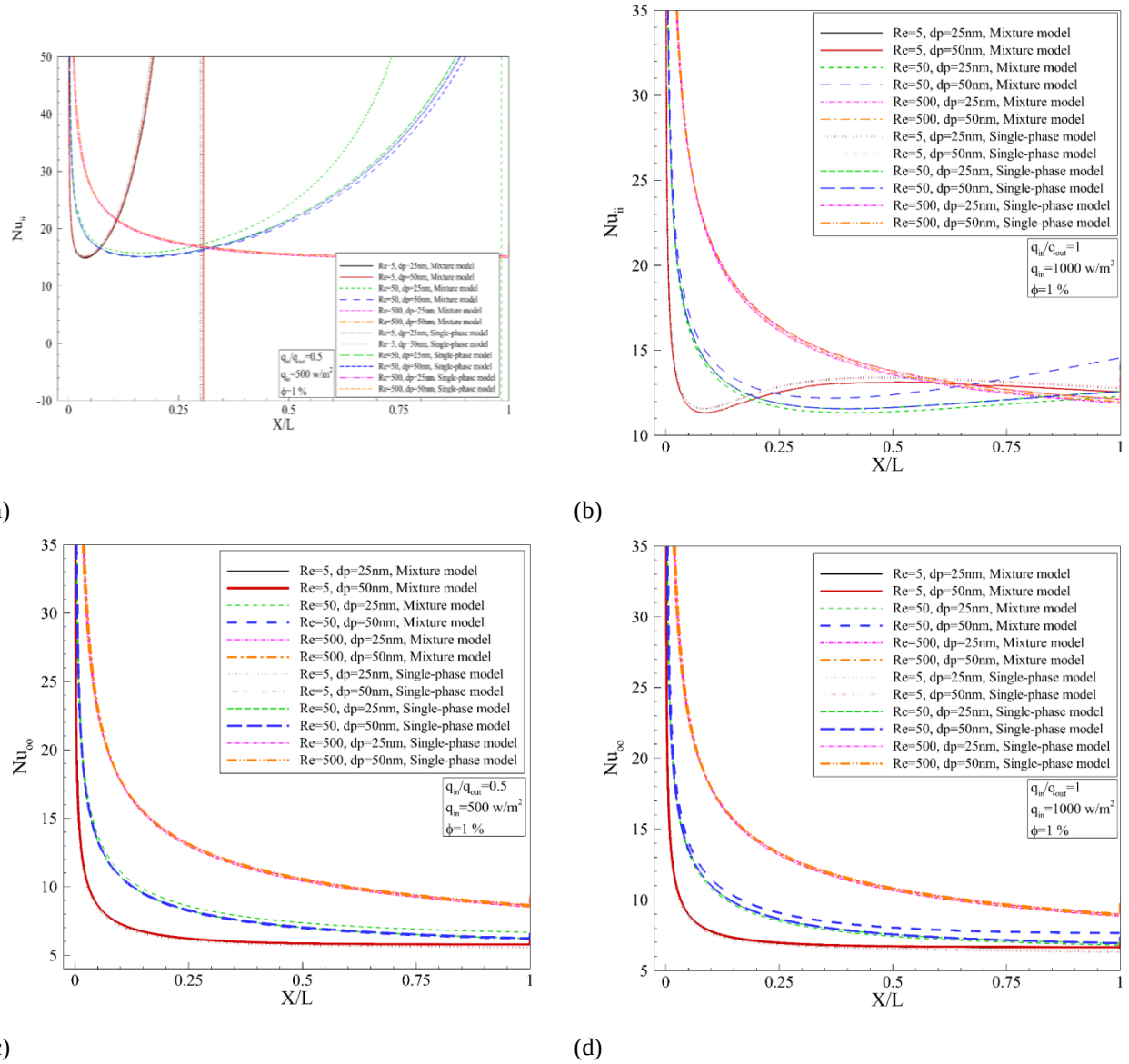

Fig. 11 Axial variations of Nu at the inner and outer tube walls for $\phi = 1\%$ and: (a, c) $q_{in}/q_{out} = 0.5$; (b, d) $q_{in}/q_{out} = 1$

where x is the axial distance.

To examine how Nu varies with effective parameters, such as Re, Pr, and ϕ, as well as by changing CMC 0.5% rheology and inlet velocity, various lengths of the developed region are determined for each scenario.

Table 3 presents Nu at the annulus walls for various values of x+ when Re = 100, q_{in}/q_{out} = 1, ϕ = 0.01, and d_p = 25nm, indicating that Nu remains constant beyond a certain value of x+, with no significant changes observed thereafter. This suggests that the flow is fully developed along the annulus. Specifically, Nu stabilizes at 14.39 and 6.68 for the inner and outer tube walls, respectively, at approximately x+= 0.22 (or x = 15.803 m) (see Fig. 12).

3.3 Mixture Model Vs. Single-Phase Model

Generally, the numerical results for non-Newtonian nanofluids using the single-phase model are closely in agreement with those obtained from the mixture multiphase model. Hydrodynamic characteristics, such as average axial velocity and flow pressure, show small differences. For instance, at Re=500 with 0.5% Al_2O_3, the mixture model provides the average axial velocity and pressure of 1.076 m/s and 2512.918 Pa, respectively, while the corresponding results for single-phase model are 1.0296 m/s and 2482.915 Pa, showing 4.3% and 1.2% difference, respectively. The drag coefficient also shows small variations. At Re=500, the mixture model values are 0.0176 and 0.0177 at ϕ=0.5% and 1.5%, respectively, compared to 0.0177 and 0.0179 estimated by the single-phase model.

Table 3 Nu* at the inner and outer walls of annulus**

x^+	Developing Region (Entrance Length) (m)	Nu_{ii}	Nu_{oo}
0.01	0.7180	12.67	9.62
0.02	1.4362	11.69	8.19
0.1،	7.1826	13.80	6.81
0.2،	14.366	14.37	6.69
0.25	17.957	14.40	6.68
0.32	22.986	14.39	6.68

* $Nu_{ii} = \frac{h_{ii}\, D_h}{k_{nf}}$, $Nu_{oo} = \frac{h_{oo}\, D_h}{k_{nf}}$ where mentioned in Eqs. (32, 33)

**Re $= 100,\ q_{in}/q_{out} = 1, \phi = 0.01, d_p = 25$ nm

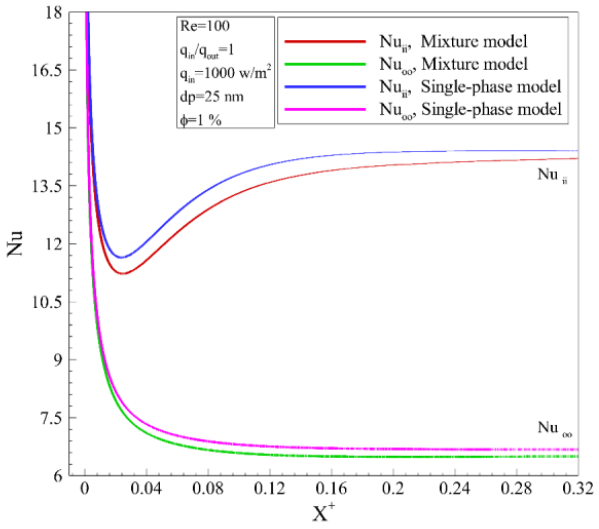

Fig. 12 Axial variation of Nu at annulus walls vs. x+ at Re = 100

The thermal characteristics can be also described. For instance, at q_{in} =1000 W/m² and Re=5, the bulk temperature in the developed region is 303.072 K and 302.943 K for ϕ=0.5% and ϕ=1.5%, respectively, when the mixture model is employed. For Re=500 and the same volume fractions, the temperatures are 300.2539 K and 300.2423 K, respectively. The single-phase model yields temperatures of 300.2532 K and 300.2411 K under similar conditions. Additionally, for Re=100, the values of Nu at the annulus inner wall is 4.59 and 4.41 by utilizing the mixture and the single-phase models, respectively, while at the annulus outer wall, these values are 3.62 and 3.53, respectively.

The consistency of the above conclusions can be extended to thermal characteristics. For instance, when $q_{in} = 1000$ W/m² and Re=5, the bulk temperatures in the developed region are 303.072 K and 302.943 K for , ϕ = 0.5% and ϕ = 1.5%, respectively, using the mixture model. For Re = 500 and the same volume fractions, the temperatures are 300.2539 K and 300.2423 K, respectively. Corresponding temperatures obtained from the single-phase model are 300.2532 K and 300.2411 K at Re = 500. Additionally, for Re = 100, Nu at the annulus inner wall is 4.59 when the mixture model is used and 4.41 when the single-phase model is employed, while at the annulus outer wall, these values are 3.62 and 3.53, respectively.

For Re=500, q_{in}/q_{out} =1, ϕ=1.5%, and dp=50nm, the bulk temperature of non-Newtonian nanofluids K at the outlet changes from 300 K at the inlet to 300.2885 using the mixture model, representing about a 0.1% enhancement. The difference between the results from the mixture and single-phase models for ϕ= 1.5 is approximately 0.4%. The maximum variation in Nu calculated using the two models is around 4%.

Thus, it can be asserted that the single-phase model used in this research yields results comparable to those obtained from the mixture model. Additionally, both models have been validated with high accuracy against experimental data.

4. CONCLUSION

This research numerically investigates the thermal behavior of CMC 0.5%/Al_2O_3, a unique non-Newtonian nanofluid with distinct rheological properties, i.e., n and K, compared to other non-Newtonian nanofluids in the developed region of an annulus. The following significant results are as follows:

- The temperature profile at the entrance of the developed region is uniform. However, as the fluid flows along the annulus, heat flux from the walls significantly alters the temperature profile, affecting the inner layers of the fluid.
- Variations in heat flux lead to significant changes in the temperature gradient (∂T/∂r) on the inner wall. These changes are intensified as heat flux increases.
- As anticipated, the temperature distribution is asymmetric when higher energy is concentrated at the outer wall.
- The bulk fluid temperature varies linearly and is slightly lower than the inner wall temperature throughout the developed region.

- Due to low inner wall-to-bulk temperature difference in the laminar flow with Re=5, unusual variations are observed in h and Nu along the annulus.
- The results indicate that, as expected, increasing Re leads to higher h and Nu.
- For the same amounts of Re, h and Nu exhibit a slight increase by enhancing nanoparticle volume fraction.
- The nanoparticle diameter has a negligible effect on the obtained results. By increasing the nanoparticle diameter from 25 nm to 50 nm, a reduction of 0.5% in h_{ii} is observed.
- The results from the studied cases show strong agreement between the single-phase model predictions and the multiphase mixture model results for non-Newtonian nanofluids. Consequently, the multiphase model is suitable for future numerical simulation in the field of CMC 0.5%/ Al_2O_3, as a non-Newtonian nanofluid.

FUNDING

The authors declare that no funds, grants, or other support were received during the preparation of this manuscript.

CONFLICTS OF INTEREST

The authors declare that there are no any conflicts of interest.

AUTHOR CONTRIBUTIONS

Farshid Marzban contributed to the conceptualization, data curation, formal analysis, investigation, methodology, resources, software, validation, visualization, and writing of the original draft. He also played a significant role in funding acquisition. **Mahshid Marzban** assisted in funding acquisition and contributed to software development. **Kazem Mohammadzadeh** was responsible for project administration and supervision, and contributed to reviewing and editing the manuscript. **Abazar Abadeh** contributed to reviewing and editing the manuscript. All authors reviewed and approved the final version of the manuscript.

REFERENCES

Abadeh, A., Davoodabadi Farahani, S., Mohammadzadeh, K., & Ghanbari, D. (2023). An experimental study on ferrofluid flow and heat transfer in a micro-fin straight circular tube. *Journal of Thermal Analysis and Calorimetry*, *148*(16), 8375–8386. https://doi.org/10.1007/s10973-023-12024-4

Ahmad Khan, S., & Altamush Siddiqui, M. (2020). Numerical studies on heat and fluid flow of nanofluid in a partially heated vertical annulus. *Heat Transfer - Asian Research*, *December 2019*. https://doi.org/10.1002/htj.21672

Akbar, N. S., Raza, M., & Ellahi, R. (2016). Copper oxide nanoparticles analysis with water as base fluid for peristaltic flow in permeable tube with heat transfer. *Computer Methods and Programs in Biomedicine*, *130*, 22–30. https://doi.org/10.1016/j.cmpb.2016.03.003

Akbari, O. A., Toghraie, D., & Karimipour, A. (2015). Impact of ribs on flow parameters and laminar heat transfer of water-aluminum oxide nanofluid with different nanoparticle volume fractions in a three-dimensional rectangular microchannel. *Advances in Mechanical Engineering*, *7*(11). https://doi.org/10.1177/1687814015618155

Akbari, O. A., Toghraie, D., Karimipour, A., Marzban, A., & Ahmadi, G. R. (2017). The effect of velocity and dimension of solid nanoparticles on heat transfer in non-Newtonian nanofluid. *Physica E: Low-Dimensional Systems and Nanostructures*, *86*, 68–75. https://doi.org/10.1016/j.physe.2016.10.013

Al-Kouz, W., Abderrahmane, A., Shamshuddin, MD., Younis, O., Mohammed, S., Bég, O. A., & Toghraie, D. (2021). Heat transfer and entropy generation analysis of water-Fe3O4/CNT hybrid magnetic nanofluid flow in a trapezoidal wavy enclosure containing porous media with the Galerkin finite element method. *The European Physical Journal Plus*, *136*(11), 1184. https://doi.org/10.1140/epjp/s13360-021-02192-3

Anoop, K. B., Sundararajan, T., & Das, S. K. (2009). Effect of particle size on the convective heat transfer in nanofluid in the developing region. *International Journal of Heat and Mass Transfer*, *52*(9–10), 2189–2195. https://doi.org/10.1016/j.ijheatmasstransfer.2007.11.063

Azmi, W. H., Sharma, K. V., Mamat, R., Alias, A. B. S., & Izwan Misnon, I. (2012). *Correlations for thermal conductivity and viscosity of water based nanofluids.* IOP Conference Series: Materials Science and Engineering. https://doi.org/10.1088/1757-899X/36/1/012029

Bahiraei, M., & Alighardashi, M. (2016). Investigating non-Newtonian nanofluid flow in a narrow annulus based on second law of thermodynamics. *Journal of Molecular Liquids*, *219*, 117–127. https://doi.org/10.1016/j.molliq.2016.03.007

Beheshti, A., Moraveji, M. K., & Hejazian, M. (2015). Comparative numerical study of nanofluid heat transfer through an annular channel. *Numerical Heat*

Transfer; Part A: Applications, *67*(1), 100–117. https://doi.org/10.1080/10407782.2014.894359

Behroyan, I., Vanaki, S. M., Ganesan, P., & Saidur, R. (2016). A comprehensive comparison of various CFD models for convective heat transfer of Al2O3 nanofluid inside a heated tube. *International Communications in Heat and Mass Transfer*, *70*, 27–37. https://doi.org/10.1016/j.icheatmasstransfer.2015.11.001

Benkhedda, M., Boufendi, T., & Touahri, S. (2018). Laminar mixed convective heat transfer enhancement by using Ag-TiO2-water hybrid Nanofluid in a heated horizontal annulus. *Heat and Mass Transfer/Waerme- Und Stoffuebertragung*, *54*(9), 2799–2814. https://doi.org/10.1007/s00231-018-2302-x

Bianco, V., Manca, O., & Nardini, S. (2010). Numerical simulation of water/ Al2O3 nanofluid turbulent convection. *Advances in Mechanical Engineering*, *2010*. https://doi.org/10.1155/2010/976254

Bozorg, M. V., Hossein Doranehgard, M., Hong, K., & Xiong, Q. (2020). CFD study of heat transfer and fluid flow in a parabolic trough solar receiver with internal annular porous structure and synthetic oil–Al2O3 nanofluid. *Renewable Energy*, *145*, 2598–2614. https://doi.org/10.1016/j.renene.2019.08.042

Chon, C. H., Kihm, K. D., Lee, S. P., & Choi, S. U. S. (2005a). Empirical correlation finding the role of temperature and particle size for nanofluid (Al 2O 3) thermal conductivity enhancement. *Applied Physics Letters*, *87*(15), 1–3. https://doi.org/10.1063/1.2093936

Chon, C. H., Kihm, K. D., Lee, S. P., & Choi, S. U. S. (2005b). Empirical correlation finding the role of temperature and particle size for nanofluid (Al2O3) thermal conductivity enhancement. *Applied Physics Letters*, *87*(15). https://doi.org/10.1063/1.2093936

Corcione, M. (2011). Empirical correlating equations for predicting the effective thermal conductivity and dynamic viscosity of nanofluids. *Energy Conversion and Management*, *52*(1), 789–793. https://doi.org/10.1016/j.enconman.2010.06.072

Davoudi, A., Daneshmand, S., Monfared, V., & Mohammadzadeh, K. (2021). Numerical simulation on heat transfer of nanofluid in conical spiral heat exchanger. *Progress in Computational Fluid Dynamics*, *21*(1), 52–63. https://doi.org/10.1504/PCFD.2021.112620

Dawood, H. K., Mohammed, H. A., & Munisamy, K. M. (2014). Heat transfer augmentation using nanofluids in an elliptic annulus with constant heat flux boundary condition. *Case Studies in Thermal Engineering*, *4*, 32–41. https://doi.org/10.1016/j.csite.2014.06.001

Dawood, H. K., Mohammed, H. A., Sidik, N. A. C., Munisamy, K. M., & Alawi, O. A. (2017). Heat transfer augmentation in concentric elliptic annular by ethylene glycol based nanofluids. *International Communications in Heat and Mass Transfer*, *82*, 29–39. https://doi.org/10.1016/j.icheatmasstransfer.2017.02.008

Ellahi, R., Hassan, M., & Zeeshan, A. (2015). Shape effects of nanosize particles in Cu - H 2O nanofluid on entropy generation. *International Journal of Heat and Mass Transfer*, *81*, 449–456. https://doi.org/10.1016/j.ijheatmasstransfer.2014.10.041

Ghanbari, S., & Javaherdeh, K. (2020). Thermal performance enhancement in perforated baffled annuli by nanoporous graphene non-Newtonian nanofluid. *Applied Thermal Engineering*, *167*. https://doi.org/10.1016/j.applthermaleng.2019.114719

Hassan, M., Marin, M., Alsharif, A., & Ellahi, R. (2018a). Convective heat transfer flow of nanofluid in a porous medium over wavy surface. *Physics Letters A*, *382*(38), 2749–2753. https://doi.org/10.1016/j.physleta.2018.06.026

Hassan, M., Marin, M., Ellahi, R., & Alamri, S. Z. (2018b). Exploration of convective heat transfer and flow characteristics synthesis by Cu–Ag/water hybrid-nanofluids. *Heat Transfer Research*, *49*(18), 1837–1848.

He, Y., Men, Y., Liu, X., Lu, H., Chen, H., & Ding, Y. (2009). Study on forced convective heat transfer of non-newtonian nanofluids. *Journal of Thermal Science*, *18*(1), 20–26. https://doi.org/10.1007/s11630-009-0020-x

Heidarshenas, A., Azizi, Z., Peyghambarzadeh, S. M., & Sayyahi, S. (2020). Experimental investigation of the particle size effect on heat transfer coefficient of Al2O3 nanofluid in a cylindrical microchannel heat sink. *Journal of Thermal Analysis and Calorimetry*, *141*(2), 957–967. https://doi.org/10.1007/s10973-019-09033-7

Heris, S. Z., Etemad, S. G., & Esfahany, M. N. (2006). Experimental investigation of oxide nanofluids laminar flow convective heat transfer. *International Communications in Heat and Mass Transfer*, *33*(4), 529–535. https://doi.org/10.1016/j.icheatmasstransfer.2006.01.005

Hojjat, M., Etemad, S. G., Bagheri, R., & Thibault, J. (2011a). Convective heat transfer of non-Newtonian nanofluids through a uniformly heated circular tube.

International Journal of Thermal Sciences, *50*(4), 525–531. https://doi.org/10.1016/j.ijthermalsci.2010.11.006

Hojjat, M., Etemad, S. G., Bagheri, R., & Thibault, J. (2011b). Laminar convective heat transfer of non-Newtonian nanofluids with constant wall temperature. *Heat and Mass Transfer/Waerme- Und Stoffuebertragung*, *47*(2), 203–209. https://doi.org/10.1007/s00231-010-0710-7

Hojjat, M., Etemad, S. G., Bagheri, R., & Thibault, J. (2011c). Turbulent forced convection heat transfer of non-Newtonian nanofluids. *Experimental Thermal and Fluid Science*, *35*(7), 1351–1356. https://doi.org/10.1016/j.expthermflusci.2011.05.003

Hojjat, M., Etemad, S. G., Bagheri, R., & Thibault, J. (2011d). Turbulent forced convection heat transfer of non-Newtonian nanofluids. *Experimental Thermal and Fluid Science*, *35*(7), 1351–1356. https://doi.org/10.1016/j.expthermflusci.2011.05.003

Jafarimoghaddam, A., Aberoumand, S., Aberoumand, H., & Javaherdeh, K. (2017). Experimental study on Cu/Oil nanofluids through concentric annular tube: A correlation. *Heat Transfer - Asian Research*, *46*(3), 251–260. https://doi.org/10.1002/htj.21210

Javadpour, A., Najafi, M., & Javaherdeh, K. (2017a). Experimental study of steady state laminar forced heat transfer of horizontal annulus tube with non-Newtonian nanofluid. *Journal of Mechanical Science and Technology*, *31*(11), 5539–5544. https://doi.org/10.1007/s12206-017-1048-6

Javadpour, A., Najafi, M., & Javaherdeh, K. (2017b). Experimental study of steady state laminar forced heat transfer of horizontal annulus tube with non-Newtonian nanofluid. *Journal of Mechanical Science and Technology*, *31*(11), 5539–5544. https://doi.org/10.1007/s12206-017-1048-6

Javadpour, A., Najafi, M., & Javaherdeh, K. (2018). Effect of magnetic field on forced convection heat transfer of a non-Newtonian nanofluid through an annulus: an experimental study. *Heat and Mass Transfer/Waerme- Und Stoffuebertragung*, *54*(11), 3307–3316. https://doi.org/10.1007/s00231-018-2361-z

Koca, H. D., Doganay, S., Turgut, A., Tavman, I. H., Saidur, R., & Mahbubul, I. M. (2018). Effect of particle size on the viscosity of nanofluids: A review. *Renewable and Sustainable Energy Reviews*, *82*, 1664-1674. https://doi.org/10.1016/j.rser.2017.07.016

Kumar, V., & Sarkar, J. (2018). Two-phase numerical simulation of hybrid nanofluid heat transfer in minichannel heat sink and experimental validation. *International Communications in Heat and Mass Transfer*, *91*, 239–247. https://doi.org/10.1016/j.icheatmasstransfer.2017.12.019

Lelea, D. (2011). The performance evaluation of Al2O3/water nanofluid flow and heat transfer in microchannel heat sink. *International Journal of Heat and Mass Transfer*, *54*(17–18), 3891–3899. https://doi.org/10.1016/j.ijheatmasstransfer.2011.04.038

Lotfi, R., Saboohi, Y., & Rashidi, A. M. (2010). Numerical study of forced convective heat transfer of nanofluids: Comparison of different approaches. *International Communications in Heat and Mass Transfer*, *37*(1), 74–78. https://doi.org/10.1016/j.icheatmasstransfer.2009.07.013

Majid, S., & Mohammad, J. (2017a). Optimal selection of annulus radius ratio to enhance heat transfer with minimum entropy generation in developing laminar forced convection of water-Al2O3 nanofluid flow. *Journal of Central South University*, *24*(8), 1850–1865. https://doi.org/10.1007/s11771-017-3593-7

Majid, S., & Mohammad, J. (2017b). Optimal selection of annulus radius ratio to enhance heat transfer with minimum entropy generation in developing laminar forced convection of water-Al2O3 nanofluid flow. *Journal of Central South University*, *24*(8), 1850–1865. https://doi.org/10.1007/s11771-017-3593-7

Manninen, M., & Taivassalo, V. (1996). On the mixture model for multiphase flow. *VTT Publications*, *288*, 3–67. https://scholar.google.com/scholar_url?url=https://www.researchgate.net/profile/Sirpa_Kallio/publication/259938456_On_the_Mixture_Model_for_Multiphase_Flow/links/54b79c6a0cf2bd04be33ad85/On-the-Mixture-Model-for-Multiphase-Flow.pdf&hl=en&sa=T&oi=gsb-ggp&c

Marin, M., Hobiny, A., & Abbas, I. (2021). Finite element analysis of nonlinear bioheat model in skin tissue due to external thermal sources. *Mathematics*, *9*(13), 1459. https://doi.org/10.3390/math9131459

Masoumi, N., Sohrabi, N., & Behzadmehr, A. (2009). A new model for calculating the effective viscosity of nanofluids. *Journal of Physics D: Applied Physics*, *42*(5). https://doi.org/10.1088/0022-3727/42/5/055501

Mirzaei, M., & Azimi, A. (2016). Heat transfer and pressure drop characteristics of graphene oxide/water nanofluid in a circular tube fitted with wire coil insert. *Experimental Heat Transfer*, *29*(2), 173–187. https://doi.org/10.1080/08916152.2014.973975

Mishra, P. C., Mukherjee, S., Nayak, S. K., & Panda, A. (2014). A brief review on viscosity of nanofluids. *International Nano Letters*, *4*(4), 109–120. https://doi.org/10.1007/s40089-014-0126-3

Moghadassi, A. R., Masoud Hosseini, S., Henneke, D., & Elkamel, A. (2009). A model of nanofluids effective thermal conductivity based on dimensionless groups. *Journal of Thermal Analysis and Calorimetry*, *96*(1), 81–84. https://doi.org/10.1007/s10973-008-9843-z

Moghari, R. M., Mujumdar, A. S., Shariat, M., F. Talebi, Sajjadi, S. M., & Akbarinia, A. (2013). Investigation effect of nanoparticle mean diameter on mixed convection Al2O3-water nanofluid flow in an annulus by two phase mixture model. *International Communications in Heat and Mass Transfer*, *49*, 25–35. https://doi.org/10.1016/j.icheatmasstransfer.2013.08.017

Mohammadzadeh, K., Khaleghi, H., Khadem Abolfazli, H. R., & Seddiq, M. (2018). Effects of gas cross-over through the membrane on water management in the cathode and anode sides of PEM fuel cell. *Journal of Applied Fluid Mechanics*, *11*(4), 861–875. https://doi.org/10.29252/jafm.11.04.28559

Mojarrad, M. S., Keshavarz, A., Ziabasharhagh, M., & Raznahan, M. M. (2014). Experimental investigation on heat transfer enhancement of alumina/water and alumina/water-ethylene glycol nanofluids in thermally developing laminar flow. *Experimental Thermal and Fluid Science*, *53*, 111–118. https://doi.org/10.1016/j.expthermflusci.2013.11.015

Mokhtari Moghari, R., Akbarinia, A., Shariat, M., Talebi, F., & Laur, R. (2011a). Two phase mixed convection Al2O3-water nanofluid flow in an annulus. *International Journal of Multiphase Flow*, *37*(6), 585–595. https://doi.org/10.1016/j.ijmultiphaseflow.2011.03.008

Mokhtari Moghari, R., Akbarinia, A., Shariat, M., Talebi, F., & Laur, R. (2011b). Two phase mixed convection Al2O3-water nanofluid flow in an annulus. *International Journal of Multiphase Flow*, *37*(6), 585–595. https://doi.org/10.1016/j.ijmultiphaseflow.2011.03.008

Moraveji, M. K., Haddad, S. M. H., & Darabi, M. (2012). Modeling of forced convective heat transfer of a non-Newtonian nanofluid in the horizontal tube under constant heat flux with computational fluid dynamics. *International Communications in Heat and Mass Transfer*, *39*(7), 995–999. https://doi.org/10.1016/j.icheatmasstransfer.2012.05.003

Naderi, B., & Mohammadzadeh, K. (2020). Numerical unsteady simulation of nanofluid flow over a heated angular oscillating circular cylinder. *Journal of Thermal Analysis and Calorimetry*, *139*(1), 721–739. https://doi.org/10.1007/s10973-019-08349-8

Nasiri, M., Etemad, S. G., & Bagheri, R. (2011a). Experimental heat transfer of nanofluid through an annular duct. *International Communications in Heat and Mass Transfer*, *38*(7), 958–963. https://doi.org/10.1016/j.icheatmasstransfer.2011.04.011

Nasiri, M., Etemad, S. Gh., & Bagheri, R. (2011b). Experimental heat transfer of nanofluid through an annular duct. *International Communications in Heat and Mass Transfer*, *38*(7), 958–963. https://doi.org/10.1016/j.icheatmasstransfer.2011.04.011

Othman, M. I. A., Said, S., & Marin, M. (2019). A novel model of plane waves of two-temperature fiber-reinforced thermoelastic medium under the effect of gravity with three-phase-lag model. *International Journal of Numerical Methods for Heat & Fluid Flow*, *29*(12), 4788–4806. https://doi.org/10.1108/HFF-04-2019-0359

Popa, C. V., Nguyen, C. T., & Gherasim, I. (2017). New specific heat data for Al2O3 and CuO nanoparticles in suspension in water and Ethylene Glycol. *International Journal of Thermal Sciences*, *111*, 108–115. https://doi.org/10.1016/j.ijthermalsci.2016.08.016

Rabby, M. I. I., Hasan, M. E., Amin, A. al, & Islam, A. K. M. S. (2019, July). *Laminar convective heat transfer in developing region of a pipe by using nanofluids.* AIP Conference Proceedings, 2121. https://doi.org/10.1063/1.5115921

Rabienataj Darzi, A. A., Farhadi, M., & Lavasani, A. M. (2016). Two phase mixture model of nano-enhanced mixed convection heat transfer in finned enclosure. *Chemical Engineering Research and Design*, *111*, 294–304. https://doi.org/10.1016/j.cherd.2016.05.019

Ragueb, H., & Mansouri, K. (2018). An analytical study of the periodic laminar forced convection of non-Newtonian nanofluid flow inside an elliptical duct. *International Journal of Heat and Mass Transfer*, *127*, 469–483. https://doi.org/10.1016/j.ijheatmasstransfer.2018.07.051

Rahimi Gheynani, A., Ali Akbari, O., Zarringhalam, M., Ahmadi Sheikh Shabani, G., Alnaqi, A. A., Goodarzi, M., & Toghraie, D. (2019). Investigating the effect of nanoparticles diameter on turbulent flow and heat transfer properties of non-Newtonian carboxymethyl cellulose/CuO fluid in a microtube. *International Journal of Numerical Methods for Heat & Fluid Flow*, *29*(5), 1699–1723. https://doi.org/10.1108/HFF-07-2018-0368

Rea, U., McKrell, T., Hu, L. wen, & Buongiorno, J. (2009). Laminar convective heat transfer and viscous pressure loss of alumina-water and zirconia-water

nanofluids. *International Journal of Heat and Mass Transfer*, *52*(7–8), 2042–2048. https://doi.org/10.1016/j.ijheatmasstransfer.2008.10.025

Sajadifar, S. A., Karimipour, A., & Toghraie, D. (2017). Fluid flow and heat transfer of non-Newtonian nanofluid in a microtube considering slip velocity and temperature jump boundary conditions. *European Journal of Mechanics, B/Fluids*, *61*, 25–32. https://doi.org/10.1016/j.euromechflu.2016.09.014

Sepehrnia, M., Mohammadzadeh, K., Veyseh, M. M., Agah, E., & Amani, M. (2022a). Rheological behavior of engine oil based hybrid nanofluid containing MWCNTs and ZnO nanopowders: Experimental analysis, developing a novel correlation, and neural network modeling. *Powder Technology*, *404*, 117492. https://doi.org/10.1016/j.powtec.2022.117492

Sepehrnia, M., Mohammadzadeh, K., Veyseh, M. M., Agah, E., & Amani, M. (2022b). Rheological behavior of engine oil based hybrid nanofluid containing MWCNTs and ZnO nanopowders: Experimental analysis, developing a novel correlation, and neural network modeling. *Powder Technology*, *404*, 117492. https://doi.org/10.1016/j.powtec.2022.117492

Shahsavar, A., Moradi, M., & Bahiraei, M. (2018). Heat transfer and entropy generation optimization for flow of a non-Newtonian hybrid nanofluid containing coated CNT/Fe3O4 nanoparticles in a concentric annulus. *Journal of the Taiwan Institute of Chemical Engineers*, *84*, 28–40. https://doi.org/10.1016/j.jtice.2017.12.029

Shojaeian, M., Karimzadehkhouei, M., & Koşar, A. (2017). Experimental investigation on convective heat transfer of non-Newtonian flows of Xanthan gum solutions in microtubes. *Experimental Thermal and Fluid Science*, *85*, 305–312. https://doi.org/10.1016/j.expthermflusci.2017.02.025

Siavashi, M., & Jamali, M. (2016a). Heat transfer and entropy generation analysis of turbulent flow of TiO 2 -water nanofluid inside annuli with different radius ratios using two-phase mixture model. *Applied Thermal Engineering*, *100*, 1149–1160. https://doi.org/10.1016/j.applthermaleng.2016.02.093

Siavashi, M., & Jamali, M. (2016b). Heat transfer and entropy generation analysis of turbulent flow of TiO2-water nanofluid inside annuli with different radius ratios using two-phase mixture model. *Applied Thermal Engineering*, *100*, 1149–1160. https://doi.org/10.1016/j.applthermaleng.2016.02.093

Siavashi, M., & Rostami, A. (2017a). Two-phase simulation of non-Newtonian nanofluid natural convection in a circular annulus partially or completely filled with porous media. *International Journal of Mechanical Sciences*, *133*(July), 689–703. https://doi.org/10.1016/j.ijmecsci.2017.09.031

Siavashi, M., & Rostami, A. (2017b). Two-phase simulation of non-Newtonian nanofluid natural convection in a circular annulus partially or completely filled with porous media. *International Journal of Mechanical Sciences*, *133*, 689–703. https://doi.org/10.1016/j.ijmecsci.2017.09.031

Siavashi, M., Bahrami, H. R. T., & Saffari, H. (2017a). Numerical investigation of porous rib arrangement on heat transfer and entropy generation of nanofluid flow in an annulus using a two-phase mixture model. *Numerical Heat Transfer; Part A: Applications*, *71*(12), 1251–1273. https://doi.org/10.1080/10407782.2017.1345270

Siavashi, M., Bahrami, H. R. T., & Saffari, H. (2017b). Numerical investigation of porous rib arrangement on heat transfer and entropy generation of nanofluid flow in an annulus using a two-phase mixture model. *Numerical Heat Transfer, Part A: Applications*, *71*(12), 1251–1273. https://doi.org/10.1080/10407782.2017.1345270

Soltani, S., Etemad, S. G., & Thibault, J. (2010). Pool boiling heat transfer of non-Newtonian nanofluids. *International Communications in Heat and Mass Transfer*, *37*(1), 29–33. https://doi.org/10.1016/j.icheatmasstransfer.2009.08.005

Tahiri, A., & Mansouri, K. (2017). Theoretical investigation of laminar flow convective heat transfer in a circular duct for a non-Newtonian nanofluid. *Applied Thermal Engineering*, *112*, 1027–1039. https://doi.org/10.1016/j.applthermaleng.2016.10.137

Vajjha, R. S., & Das, D. K. (2009). Experimental determination of thermal conductivity of three nanofluids and development of new correlations. *International Journal of Heat and Mass Transfer*, *52*(21–22), 4675–4682. https://doi.org/10.1016/j.ijheatmasstransfer.2009.06.027

Vlase, S., Stac, C. N., & Marin, M. (2017). A method for the study of the vibration of mechanical bars systems with symmetries. *Acta Technica Napocensis Series*, *60*(4), 539–544.

Wen, D., & Ding, Y. (2004). Experimental investigation into convective heat transfer of nanofluids at the entrance region under laminar flow conditions. *International Journal of Heat and Mass Transfer*, *47*(24), 5181–5188. https://doi.org/10.1016/j.ijheatmasstransfer.2004.07.012

Yarmohammadi, S., Mohammadzadeh, K., Farhadi, M., Hajimiri, H., & Modir, A. (2020). Multi-objective optimization of thermal and flow characteristics of R-404A evaporation through corrugated tubes. *Journal of Energy Storage*, *27*(August 2019), 101137. https://doi.org/10.1016/j.est.2019.101137

Zarringhalam, M., Karimipour, A., & Toghraie, D. (2016). Experimental study of the effect of solid volume fraction and Reynolds number on heat transfer coefficient and pressure drop of CuO–Water nanofluid. *Experimental Thermal and Fluid Science*, *76*, 342–351. https://doi.org/10.1016/j.expthermflusci.2016.03.026

Zeinali Heris, S., Nasr Esfahany, M., & Etemad, S. G. (2007a). Experimental investigation of convective heat transfer of Al2O3/water nanofluid in circular tube. *International Journal of Heat and Fluid Flow*, *28*(2), 203–210. https://doi.org/10.1016/j.ijheatfluidflow.2006.05.001

Zeinali Heris, S., Nasr Esfahany, M., & Etemad, S. G. (2007b). Experimental investigation of convective heat transfer of Al2O3/water nanofluid in circular tube. *International Journal of Heat and Fluid Flow*, *28*(2), 203–210. https://doi.org/10.1016/j.ijheatfluidflow.2006.05.001

Zeinali Heris, S., Nasr Esfahany, M., & Etemad, S. Gh. (2007c). Experimental investigation of convective heat transfer of Al2O3/water nanofluid in circular tube. *International Journal of Heat and Fluid Flow*, *28*(2), 203–210. https://doi.org/10.1016/j.ijheatfluidflow.2006.05.001